Colloidal Inks for Directed Assembly of 3-D Periodic Structures

James E. Smay,[†,‡] Joseph Cesarano III,[‡] and Jennifer A. Lewis*[,†]

Materials Science and Engineering Department, University of Illinois at Urbana-Champaign, Urbana, Illinois 61801, and Sandia National Laboratories, Albuquerque, New Mexico 87106

Received March 8, 2002. In Final Form: May 31, 2002

Mesoscale periodic structures have been fabricated via directed assembly of colloidal inks. Concentrated colloidal gels with tailored viscoelastic properties were designed to form self-supporting features. The inks were deposited in a layer-by-layer sequence to directly write the desired 3-D pattern. Periodic structures with spanning features that vary between ~100 μm and 1 mm were assembled. Shear rate profiles were calculated on the basis of the measured rheological properties of the inks under slip and no-slip boundary conditions during flow through a cylindrical deposition nozzle. Deflection measurements of spanning elements were used to probe the relationship between gel strength, deposition speed, and shear rate profiles in the nozzle. These observations revealed that the ink adopted a rigid (gel) core−fluid shell architecture during assembly, which simultaneously facilitated bonding and shape retention of the deposited elements.

Introduction

Three-dimensional periodic structures fabricated from colloidal "building blocks" may find widespread technological application as advanced ceramics,[1,2] sensors,[3,4] composites,[5,6] and tissue engineering scaffolds.[7] These applications require both functional materials, such as those exhibiting ferroelectricity, high strength, or biocompatibility, and periodicity engineered at length scales (approximately several micrometers to millimeters) far exceeding colloidal dimensions. Direct-write techniques[8−17] offer a powerful route for producing complex 3-D structures, including space-filling solids, and structures with high aspect ratio walls or spanning (unsupported) elements. The latter structure, which exhibits the desired 3-D periodicity, places the most stringent demands on ink design.

Direct-write techniques such as robocasting,[12−14] ink jet printing,[9] hot-melt printing,[10] three-dimensional printing,[15] micropen writing,[11] and fused deposition[17] employ inks that solidify either by liquid evaporation or a temperature-induced phase change. Because of their initial fluidity, such inks are incapable of fully supporting their own weight during assembly. Robocasting[12−14] is unique among these processes because it involves the robotic deposition of highly concentrated colloidal suspensions. In prior efforts, robocasting inks were designed to solidify via a drying-induced pseudoplastic to dilatent transition.[12−14,18] Such inks were suitable for producing space-filling solids;[18] however, difficulty in controlling drying kinetics limited their applicability to forming spanning structures.

Colloidal inks developed for robotic deposition of 3-D periodic structures with spanning features must satisfy two important criteria. First, they must exhibit a well-controlled viscoelastic response; that is, they must be able to flow through a deposition nozzle and then "set" immediately to facilitate shape retention of the deposited features even as they span gaps in the underlying layer(s). Second, they must contain high colloid volume fractions to minimize drying-induced shrinkage after assembly; that is, the particle network must be able to resist compressive stresses arising from capillary tension.[19] These criteria require careful control of colloidal forces to first generate a highly concentrated, stable dispersion and then induce a system change (e.g., ΔpH, ionic strength, or solvent quality) that promotes a fluid-to-gel transition.

Colloidal gels consist of a percolating network of attractive particles capable of transmitting stress above a critical volume fraction (ϕ_{gel}), known as the gel point. In our approach, the colloid volume fraction (ϕ) within the gelled ink is held constant, while its elastic properties are tuned by tailoring the strength of the interparticle

* Corresponding author. E-mail: jalewis@uiuc.edu.
† University of Illinois at Urbana-Champaign.
‡ Sandia National Laboratories.

(1) Lewis, J. A. *J. Am. Ceram. Soc.* **2000**, *83* (10), 2341−59.
(2) Tohver, V.; Smay, J. E.; Bream, A.; Braun, P. V.; Lewis, J. A. *PNAS* **2001**, *98*, 8950−54.
(3) Allahverdi, M.; Danforth, S. C.; Jafari, M.; Safari, A. *J. Eur. Ceram. Soc.* **2001**, *21* (10−11), 1485−90.
(4) Tressler, J. F.; Alkpu, S.; Dogan, A.; Newnham, R. E. *Composites, Part A: Appl. Sci. Manuf.* **1999**, *30A* (4), 477−82.
(5) Soundararajan, R.; Kuhn, G.; Atisivan, R.; Bose, S.; Bandyopadhyay, A. *J. Am. Ceram. Soc.* **2001**, *84* (3), 509−13.
(6) Rao, M. P.; Sanchez-Herencia, A. J.; Beltz, G. E.; McMeeking, R. M.; Lange, F. F. *Science* **1999**, *286*, 102−105.
(7) Chu, T. M.; Halloran, J. W.; Hollister, S. J.; Feinberg, S. E. *J. Mater. Sci.: Mater. Med.* **2001**, *12*, 471−78.
(8) Chrisey, D. B. *Science* **2000**, *289* (5481), 879−881.
(9) Song, J. H.; Edirisinghe, M. J.; Evans, J. R. G. *J. Am. Ceram. Soc.* **1999**, *82* (12), 3374−80.
(10) Seerden, K. A. M.; Reis, N.; Evans, J. R. G.; Grant, P. S.; Halloran, J. W.; Derby, B. *J. Am. Ceram. Soc.* **2001**, *84* (11), 2514−20.
(11) Morissette, S. L.; Lewis, J. A.; Clem, P. G.; Cesarano, J., III; Dimos, D. B. *J. Am. Ceram. Soc.* **2001**, *84* (11), 2462−68.
(12) Cesarano, J., III; Calvert, P. Freeforming Objects with Low-Binder Slurry. US Patent 6,027,326.
(13) Cesarano, J., III; Segalman, R.; Calvert, P. *Ceram. Ind.* **1998**, *148* (4), 94−102.
(14) Cesarano, J., III. *Mater. Res. Soc. Symp. Proc.: Solid Freeform and Additive Fabrication* **1998**, *542*, 133−139.
(15) Sachs, E.; Cima, M.; WIlliams, P.; Brancazio, D.; Cornie, J. *J. Eng. Ind.−Trans. ASME* **1992**, *114* (4), 481−488.
(16) Sachs, E.; Cima, M.; Bredt, J.; Curodeau, A.; Fan, T.; Brancazio, D. *Manufact. Rev.* **1992**, *5* (2), 117−26.
(17) Agarwala, M.; Bandyopadhyay, A.; van Weewn, R.; Safari, A.; Danforth, S. C.; Langrana, N. A.; Jamalabad, V. R.; Whalen, P. J. *Am. Ceram. Soc. Bull.* **1996**, *75* (11), 60−66.
(18) Tuttle, B. A.; Smay, J. E.; Cesarano, J., III; Voigt, J. A.; Scofield, T. W.; Olson, W. R. *J. Am. Ceram. Soc.* **2001**, *84* (4), 872−874.
(19) Guo, J. J.; Lewis, J. A. *J. Am. Ceram. Soc.* **1999**, *82* (9), 2345−58.

10.1021/la0257135 CCC: $22.00
Published on Web 06/14/2002

attractions according to the scaling relationship[20] given by

$$y = k\left(\frac{\phi}{\phi_{gel}} - 1\right)^x \quad (1)$$

where y is the elastic property of interest (shear yield stress (τ_y) or elastic modulus (G')), k is a constant, and x is the scaling exponent (~2.5). The equilibrium mechanical properties of colloidal gels are governed by two parameters: ϕ, which is proportional to their bond density, and ϕ_{gel}, which scales inversely with bond strength. As the interparticle forces are made more attractive, colloidal gels (of constant ϕ) experience significant increases in their elastic properties.[20−28]

Here, the effects of rheological properties and deposition conditions on the shape evolution of colloidal gel-based inks used in the directed assembly of 3-D periodic structures containing spanning elements were studied. Shear viscometry and oscillatory measurements were carried out to characterize the flow behavior and elastic properties of highly concentrated inks of varying gel strength. Colloidal ink dynamics and the shape evolution of spanning elements were determined from systematic deflection measurements. These observations highlight the robustness of this gel-based ink approach and the applicability of the analysis in predicting shape evolution. This approach opens up an unexplored route for the directed assembly of complex 3-D periodic lattices and radial arrays.

Experimental Section

Materials Systems. Lead zirconate titanate (PZT) (PZT-5H, Morgan Matroc, Electro Ceramics Division, Bedford, OH), a ferroelectric material, with a density of 7.59 g/cm^3, specific surface area of 1.86 m^2/g, and average particle size of 0.64 μm and size ranging from 0.2 to 5 μm served as the colloidal phase. The as-received PZT particles, which contained ~0.3 wt % poly(acrylic acid) preadsorbed as a dispersant, were suspended in an aqueous solution of 0.5 wt % cellulose (Methocel F4M, DOW Chemical Co., Midland, MI) in deionized water. The pH was adjusted by titration of NH_4OH and HNO_3 (reagent grade, Fisher Scientific).

Concentrated Colloidal Gels. Concentrated colloidal gels were produced by first adding an appropriate volume fraction of PZT powder (ϕ_{PZT}) to deionized water that had been preadjusted to pH ~ 10.35 with NH_4OH. Under these pH conditions, a stable suspension (ϕ_{PZT} = 0.55) was formed. The suspension was vigorously agitated for 10 min followed by sonication (XL2020 Sonicator, Misonix Inc., Farmingdale, NY) for 5 min with a 1 s on/off pulse sequence and a power of ~150 W. The suspension was then gently shaken for 1 h before and after adding an aliquot of an aqueous cellulose stock solution. Particle gelation was induced by lowering the pH via HNO_3 titration. Finally, the colloidal gel (ϕ_{PZT} = 0.47 and cellulose concentration of 5 mg/mL) was vigorously shaken for 1 h and its pH was measured with a liquid junction electrode (Ross Sure-flow Combination Electrode Model 81-65, Thermo Orion, Inc., Beverly, MA).

Rheological Measurement of Concentrated Colloidal Gels. The rheological properties of concentrated colloidal gels were characterized using a controlled stress rheometer (Bohlin Rheologi CS-10, East Brunswick, NJ) fitted with a concentric cylinder (C14, bob diameter of 14 mm and gap width of 0.7 mm) or vane tool (V25, vane diameter of 25 mm and gap width of 1.25 mm) geometry. Their apparent viscosity (η_{app}) was measured in stress viscometry mode using the concentric cylinder geometry, which has a stress range of 0.14 to 1400 Pa with a lower shear rate limit of 0.05 s^{-1}. Shear rate ($\dot{\gamma}$) data were acquired as a function of shear stress (τ) in an ascending series of discrete steps with a 1 min equilibration time at each stress. Their elastic shear modulus (G') was measured in oscillatory mode using the vane tool, which has a stress range of 0.025 to 246 Pa, a strain sensitivity of ~10^{-4}, and suitable geometry for these sensitive measurements.[29] G' was measured by performing a stress sweep at a frequency of 1 Hz. The stress sweep was repeated several times after observing a quiescent equilibration time of ~1 h between measurements. All measurements were performed at 25 °C using a specially designed solvent trap filled with deionized water to minimize evaporation.

Robotic Deposition. Mesoscale test structures, periodic lattices, and radial arrays were fabricated using a robotic deposition apparatus (Robocaster, Sandia National Laboratories, Albuquerque, NM). This directed assembly technique employs an ink delivery system mounted on a z-axis motion control stage for agile printing onto a moving $x-y$ stage. Three-axis motion was independently controlled by a custom-designed, computer-aided direct-write program (RoboCAD 2.0) that allowed for the construction of complex, 3-D architectures in a layerwise deposition scheme. The ink was housed in a syringe (barrel diameter = 4.6 mm, EFD Inc., East Providence, RI) and deposited through a cylindrical nozzle (diameter, D = 100 μm to 1 mm, and length = 14 mm) at a volumetric flow rate (=$0.25\pi D^2 v$) required to maintain a constant $x-y$ table speed (v). The deposition process was carried out under a nonwetting oil to prevent drying during assembly.

V-shaped test structures were assembled (D = 200 μm, v = 2−8 mm/s) consisting of a support base, a spanning layer, and a marker layer, as illustrated in Figure 1. The support base was deposited in the form of two isosceles triangles, one inside the other. The outer triangle had a vertex angle of 30° whereas the inner triangle had a vertex angle of 15°. Both shared a collinear perpendicular bisector of the vertex. On top of these two triangles, an array of spanning elements (rods) was deposited parallel to the base of the triangle(s). Thus, the span distance (L) across the inner triangle was systematically varied according to the simple geometric relationship

$$L = 2x \tan(7.5°) \quad (2)$$

where x is the distance from the vertex. Next, a marker layer was deposited atop the spanning layer in the same pattern as that for the support base to aid in visualizing L. A layer spacing Δz of 0.82D was used to promote intimate contact between layers.

All V-shaped test structures were assembled in a nonwetting oil bath and allowed to rest undisturbed in this bath for 30 min after deposition was completed. This procedure was adopted to eliminate the effects of nonuniform drying during the deposition process. Spanning elements deposited from the weakest gel-based ink were observed to deform over a 1−2 s period after initial deposition. The 30 min aging period was therefore deemed sufficient for the elements to achieve their equilibrium shape. After aging, the oil was slowly drained and the test structures were dried under ambient conditions (~30% relative humidity, $T \approx$ 23 °C).

Mesoscale periodic lattices were assembled (D = 200−400 μm, v = 6 mm/s, Δz = 0.82D), which consisted of a linear array of rods aligned with the x- or y-axis such that their orientation was orthogonal to the previous layer. The rod spacing (L) varied from 300 to 1200 μm when using the 200 μm nozzle and was fixed at 1210 μm when using the 400 μm nozzle. Radial arrays were also assembled (D = 200 μm, v = 6 mm/s, Δz = 0.82D) by the sequential deposition of layers with alternating patterns of concentric rings

(20) Channell, G. M.; Zukoski, C. F. *AIChE J.* **1997**, *43* (7), 1700−1708.
(21) Rueb, C. J.; Zukoski, C. F. *J. Rheol.* **1997**, 197−218.
(22) Buscall, R.; Mills, P. D. A.; Goodwin, J. W.; Lawson, D. W. *J. Chem. Soc., Faraday Trans. 1* **1988**, *84* (12), 4249−4260.
(23) Grant, M. C.; Russel, W. B. *Phys. Rev. E* **1993**, *47* (4), 2606−14.
(24) Russel, W. B. *J. Rheol.* **1980**, *24* (3), 287−317.
(25) Shih, W. Y.; Shih, W.-H.; Aksay, I. A. *J. Am. Ceram. Soc.* **1999**, *82* (3), 616−24.
(26) Shih, W.-H.; Shih, W. Y.; Kim, S.-I.; Liu, J.; Aksay, I. A. *Phys. Rev. A* **1990**, *42* (8), 4772−4779.
(27) Shih, W.-H.; Liu, J.; Shih, W. Y.; Kim, S. I.; Sarikaya, M.; Aksay, I. A. *Mater. Res. Soc. Symp. Proc.* **1989**, *155*, 83−92.
(28) Sonntag, R. C.; Russel, W. B. *J. Colloid Interface Sci.* **1987**, *116* (2), 485−489.
(29) Dzuy, N. Q.; Boger, D. V. *J. Rheol.* **1985**, *29* (3), 335−47.

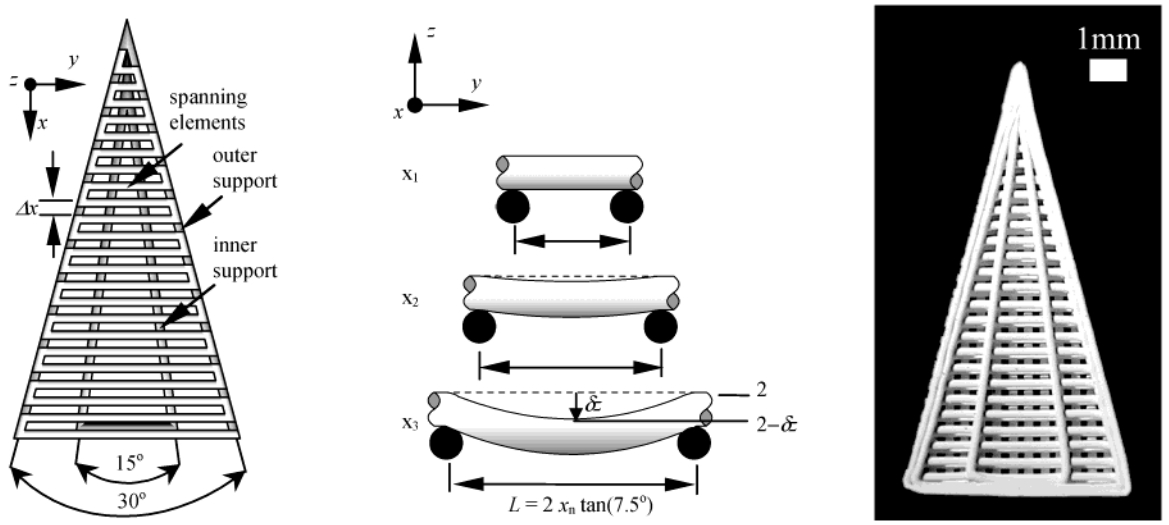

Figure 1. (a) Schematic top view of V-shaped test structure highlighting the inner and outer support structures and spanning elements (marker layer is not shown). (b) Illustration of select spans demonstrating the reference height of 2 mm and the variation of span length (L) between the inner supports as a function of x position. (c) Top view of a dried V-shaped test structure assembled at a 6 mm/s deposition speed from the strongest gel-based ink (pH = 6.15).

and a circular array of radially oriented rods. The first layer was an array of five equally spaced concentric rings between an inner and outer diameter of 3.8 and 9.7 mm, respectively. In the second layer, an array of radially oriented rods was deposited between the inner and outer radii. The angular spacing between the rods was 4.68°, such that the arc length between adjacent rods varied from 0.38 to 0.19 mm moving from the outer to inner radius.

The periodic lattices and radial arrays were removed from the oil bath after assembly and dried under ambient conditions. They were then densified by high-temperature sintering to a density of ~7.5 g/cm^3, thus reducing the porosity in the rods to ~1%. The time−temperature schedule was 3 °C/min to 600 °C, hold for 2 h, 3 °C/min to 1275 °C, hold for 2 h, and 3 °C/min to room temperature. Following densification, the periodic lattice was cut with a diamond saw at a 45° angle through the intersections between layers to reveal the internal structure.

Shape Evolution of Spanning Elements. The ability of spanning elements (rods) of the gel-based ink to withstand gravity-induced deformation was studied via measuring their deflection profiles with noncontact, laser profilometry (Model 301K, Keyence Co., Osaka, Japan). The V-shaped test structures allowed for a systematic analysis of rod deflection as a function of span distance. The profilometer employs a digital triangulation sensor that projects a 670 nm, 0.95 mW laser on the test object and calculates the distance from a reference point by determining the position of diffuse reflected light on a pixelized-array detector. The laser spot diameter was nominally 30 μm throughout the working focal range of ±5 mm with ~10 μm distance resolution. A computer-controlled $x-y$ translation stage was used to raster the laser over a rectangular area (10.5 × 6 mm^2), capturing height information for the entire test structure with a 10 × 10 μm^2 grid spacing. A reference height of 2 mm was assigned to the top surface of the spanning elements directly above their inner support, such that their deflection *(δz)* is represented by a height $z = (2 - \delta z)$. A total scanning time of 12 h was required for each test structure.

Results

Viscoelastic Behavior of Concentrated Colloidal Inks. The rheological behavior of concentrated PZT inks exhibited a strong dependence on pH. Above pH ~ 8.5, PZT suspensions were stable and displayed shear thinning behavior without a yield stress. Such suspensions underwent a fluid-to-gel transition upon reducing their pH. Their apparent viscosity as a function of pH is shown in Figure 2. Each ink displayed marked shear thinning behavior with η_{app} increasing as pH decreased. Their elastic modulus as a function of stress amplitude and pH is shown in Figure 3. Within the linear viscoelastic region, these curves displayed a well-defined equilibrium modulus, G'_{eq}, which exhibited a 5-fold increase over the pH range probed, indicative of the dramatic rise in gel strength with decreasing pH. The yield stress (τ_y) was coincident with the rapid decline of G' observed with increasing shear stress. τ_y was evaluated at $G' = 0.9G'_{eq}$[21] and found to increase from approximately 3 to 25 Pa with decreasing pH. These data are summarized in Table 1.

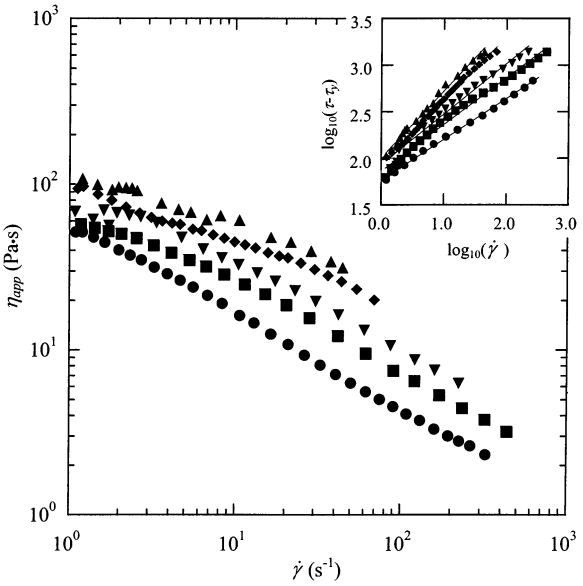

Figure 2. Apparent viscosity (η_{app}) as a function of shear rate ($\dot{\gamma}$) for colloidal inks of varying pH = 8.05 (●), 7.6 (■), 7.2 (▼), 6.85 (◆), and 6.15 (▲). The inset is a linear plot of $\log_{10}(\tau - \tau_y)$ as a function of $\log_{10}(\dot{\gamma})$ for these gel-based inks. The lines are linear fits of the experimental data used to extract the Hershel−Bulkley viscosity parameter and shear thinning exponent values reported in Table 1.

Shape Evolution of Spanning Elements. The height profiles of V-shaped test structures assembled from

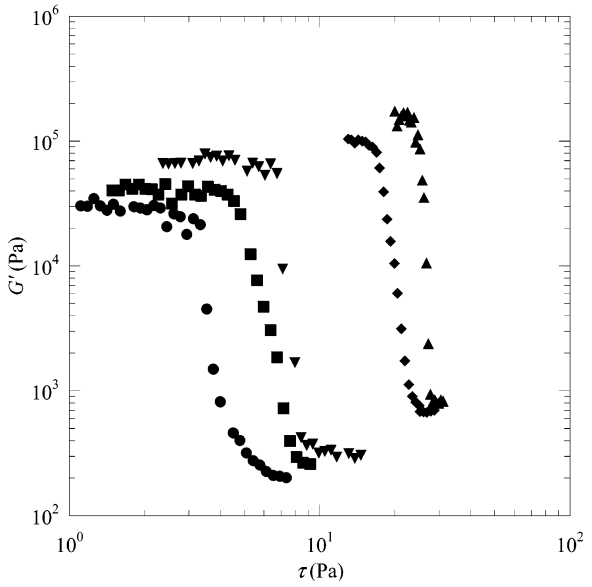

Figure 3. log−log plot of storage modulus (G') as a function of increasing stress amplitude (τ) applied at 1 Hz for colloidal inks of varying pH = 8.05 (●), 7.6 (■), 7.2 (▼), 6.85 (◆), and 6.15 (▲).

Table 1. Rheological Properties of Colloidal Inks

pH	G'_{eq} (kPa)	τ_y (Pa)	K (Pa·s^n)	n
6.15	150	25.0	101	0.72
6.85	100	16.0	86	0.68
7.20	67	6.8	76	0.57
7.60	40	4.8	72	0.50
8.05	27	3.0	58	0.44

colloidal inks of varying gel strength are shown in Figure 4a−d. The color scale representing height data was limited to a range from 1.8 to 2 mm, such that values arising from the marker layer above or severely slumped rods below this range were not displayed. The maximum rod deflection occurred midway between the inner supports and increased with span length (L = 0.53 mm at the apex of the structure to L = 2.60 mm at the base of the triangular support). Representative spans were selected from each test structure, and their height profiles were plotted as a function of position between the inner supports in Figure 4e−h. Test structures assembled from the weakest ink experienced severe deformation even at modest span lengths, whereas those assembled from the strongest ink exhibited maximum deflections less than 0.25D for spanning distances up to 2 mm. The height profiles of test structures deposited from the strongest ink at varying deposition speeds are shown in Figure 5a and b, respectively. Representative profiles plotted as a function of position in Figure 5c and d revealed that deposition speed only had a minor effect on spanning behavior for the conditions studied.

Robotic Deposition of Periodic Structures. 3-D periodic lattices and radial arrays assembled from the strongest gel-based ink are shown in Figure 6a and b, respectively. The lattice structure has tetragonal symmetry with a planar filling fraction of $\Gamma_p = 0.33$, where Γ_p is defined as the ratio D/L. The representative radial array shown in Figure 6b has cylindrical symmetry, where Γ_p in the radially oriented layer varied from 0.85 to 0.4 from the inner to outer radius. The top layer is an array of radial lines, and the underlying layer is a series of concentric rings. The rings maintained their circular shape during deposition despite the changing arc length between supports provided by the radial lines in the previous layer. The deposited rods maintained a circular cross section and spanned the gaps in underlying layers with minimal deflection. High integrity interfaces were formed between the layers by fusion of the lattice rods at junctions, as observed in Figure 7. These junctions strengthened the structures so they could be easily handled after densification. Their surface roughness illustrated in Figure 7c was governed by the characteristic grain size (approximately a few microns) in the densified structure.

Discussion

The directed assembly of 3-D periodic structures containing spanning elements required the design of concentrated colloidal-gel based inks. Such inks must flow through the deposition nozzle and then quickly "set" to maintain their shape while simultaneously bonding to the underlying layer. The shear rate profiles experienced by the ink during deposition are discussed first, followed by a discussion of the shape evolution of spanning elements after deposition. Finally, the implications of these observations on colloidal ink design for robotic deposition are addressed.

Flow through the Deposition Nozzle. The shear rheology of these concentrated colloidal inks can be described by the Hershel−Bulkley model:[30]

$$\tau = \tau_y + K\dot{\gamma}^n \tag{3}$$

where n is the shear thinning exponent and K is the viscosity parameter. These parameters, obtained by fitting the curves of $\log_{10}(\tau - \tau_y)$ versus $\log_{10}(\dot{\gamma})$ shown in the inset of Figure 2, are summarized in Table 1. The ink flows through a capillary when a pressure gradient ΔP is applied along the length (l), and a radially varying shear stress (τ_r) develops:

$$\tau_r = \frac{r\Delta P}{2l} \tag{4}$$

where r is the radial position within the nozzle (i.e., r = 0 at the center axis and $r = R$ at the nozzle wall). The shear rate profile can therefore be calculated from the constitutive relationship given by eq 3 and the applied stress field given by eq 4.

A Hershel−Bulkley material flowing through a cylindrical nozzle may adopt a three-zone velocity profile, consisting of (1) an unyielded core of radius r_c moving at constant velocity surrounded by (2) a yielded shell experiencing laminar flow and, possibly, (3) slip at the nozzle wall.[31−39] The term slip refers to the development of a thin fluid layer between the nozzle wall and the colloidal ink, whose thickness (δ) ≪ R. The volumetric flow rate (Q) as a function of applied pressure is found by

(30) Herschel, W. H.; Bulkley, R. *Kolloid Z.* **1926**, *39*, 291.
(31) Buscall, R.; McGowan, J. I.; Morton-Jones, A. J. *J. Rheol.* **1993**, *37* (4), 621−641.
(32) Cameron, J. R. *J. Rheol.* **1989**, *33* (1), 15−46.
(33) Huzzard, R. J.; Blackburn, S. *Powder Technol.* **1998**, *97*, 118−123.
(34) Kahn, A. U.; Briscoe, B. J.; Luckham, P. F. *J. Eur. Ceram. Soc.* **2001**, *21*, 483−491.
(35) Kalyon, D. M.; Yaras, P.; Aral, B.; Yilmazer, U. *J. Rheol.* **1993**, *37* (1), 35−53.
(36) Reed, J. S. *Principles of Ceramics Processing*, 2nd ed.; John Wiley and Sons: New York, 1995.
(37) Van Vazer, J. R.; Lyons, J. W.; Kim, K. Y.; Colwell, R. E. *Viscosity and Flow Measurement*; Interscience Publishers: New York, 1963.
(38) Yaras, P.; Kalyon, D. M.; Yilmazer, U. *Rheol. Acta* **1994**, *33*, 48−59.
(39) Yilmazer, U.; Kalyon, D. M. *J. Rheol.* **1989**, *33* (8), 1197−1212.

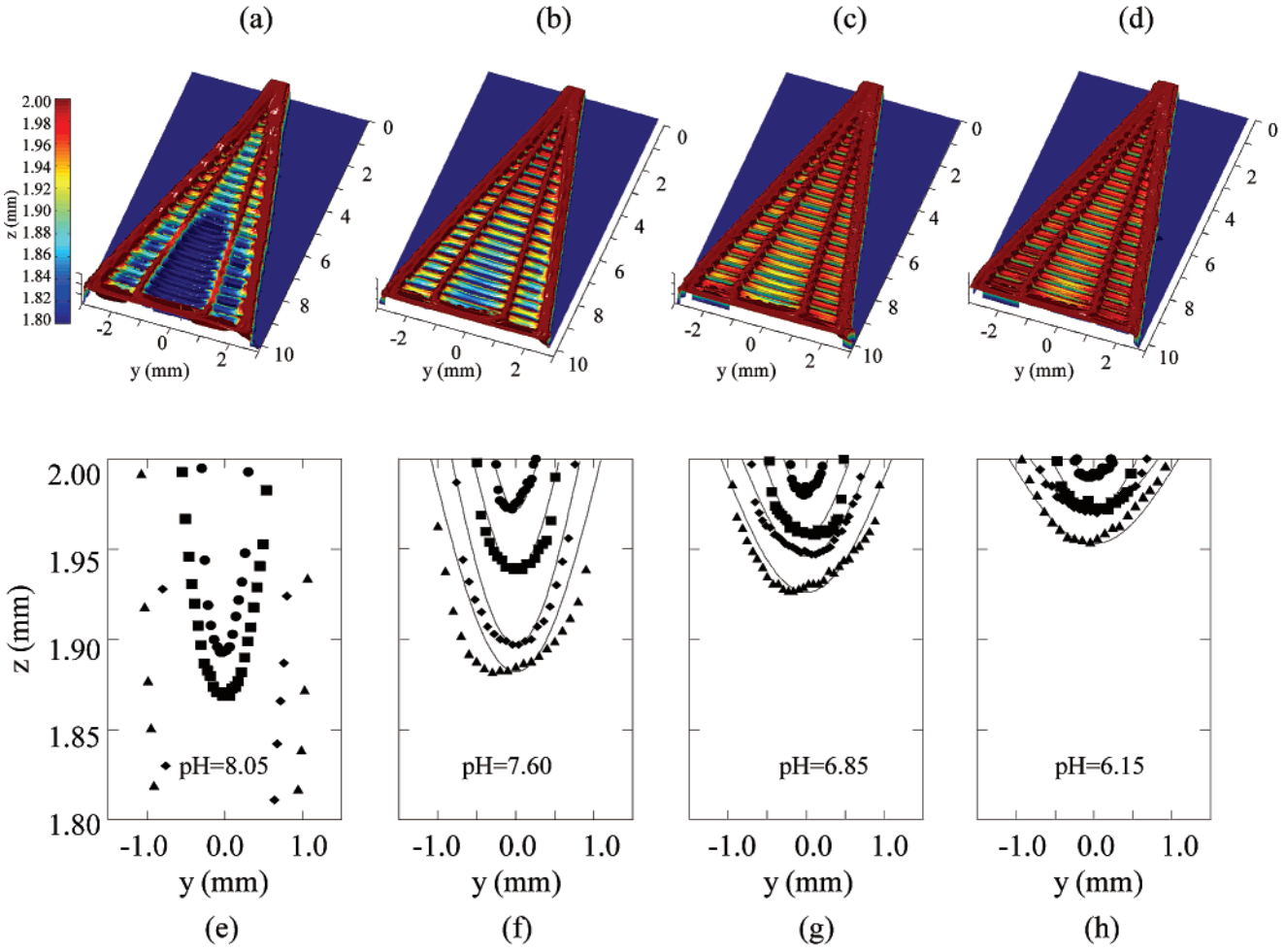

Figure 4. (a−d) Height profiles of test structures deposited from colloidal gels of varying pH = (a) 8.05, (b) 7.60, (c) 6.85, and (d) 6.15 where the color scale represents heights between 1.8 and 2 mm. (e−h) Select height profiles for spans at approximate *x* positions of 3 (●), 5 (■), 7 (◆), and 9 (▲) mm from colloidal inks at varying pH = (e) 8.05, (f) 7.60, (g) 6.85, and (h) 6.15. The lines in parts e−h are generated from a simply supported beam with distributed load model.

summing the contributions from slip at the nozzle wall and the integrated velocity profile in the core−shell region:

$$Q = \pi R^2(v_s + f(\tau_s)) \tag{5}$$

where v_s is the slip velocity and $f(\tau_r)$ is the integrated velocity profile of the core and shell region. The slip velocity is determined by

$$v_s = \frac{(\tau_R^4 - \tau_s^4)}{4\tau_R^3\eta_c} \tag{6}$$

where τ_R is the shear stress at the nozzle wall, τ_s is the shear stress at the slip layer−gel interface, and $\eta_c = 30$ mPa·s.[40] The function $f(\tau_r)$ is given by

$$f(\tau_s) = \frac{R\alpha^{m+1}}{m+1}\left(\frac{\tau_s}{K}\right)^m\left(\frac{\tau_s}{\tau_R}\right)\left[1 - \frac{2\alpha}{m+2} + \frac{\alpha^2}{(m+2)(m+3)}\right] \tag{7}$$

where $m = 1/n$, n is the Hershel−Bulkley shear thinning exponent, K is the viscosity parameter, $\alpha = (1 - \tau_y/\tau_s)$, and τ_y is the gel yield stress. These material parameters were used to calculate a pressure gradient required for a desired flow rate (or deposition speed) using eqs 5−7 while the shear rate profile within the nozzle was derived from eqs 3 and 4. Under the no-slip boundary condition ($\delta = 0$), eq 7 reduces to the Buckingham−Reiner[37,41] relationship for an ideal Bingham fluid or the Hagan−Poiseuille[37,41] relationship for a Newtonian fluid.

The shear rate profiles were calculated at varying deposition speeds under slip and no-slip boundary conditions, where the slip layer thickness was taken as the mean particle diameter. Shear rate profiles calculated for inks of varying gel strength and constant deposition speed are shown in Figure 8a, where the abscissa is the reduced radial position within the nozzle, r/R. The no-slip boundary condition (solid curves) resulted in a shear rate at the nozzle wall ($\dot{\gamma}_{wall}$) of ∼300 s^{-1} irrespective of gel strength. The rate of $\dot{\gamma}$ decay from the nozzle wall to the center decreased as gel strength increased. A core region existed close to nozzle axis, which is not visible on this scale. The introduction of the slip layer (dashed curves) led to a dramatic reduction in the wall shear rate (∼4 to 35 s^{-1}) and an expanded core region ($r_c/R \sim 0.035-0.1$). Shear rate profiles calculated for the strongest gel are plotted in Figure 8b as a function of deposition speed. The no-slip boundary condition (solid curves) resulted in a $\dot{\gamma}_{wall}$ ranging between 100 and 400 s^{-1} for deposition speeds from 2 to 8 mm/s, respectively. No core region was apparent except

(40) Smay, J. E.; Lewis, J. A. *J. Am. Ceram. Soc.* **2001**, *84* (11), 2495−500.

(41) Hunter, R. J. *Foundations of Colloid Science*; Oxford University Press Inc.: New York, 1992; Vol. 2.

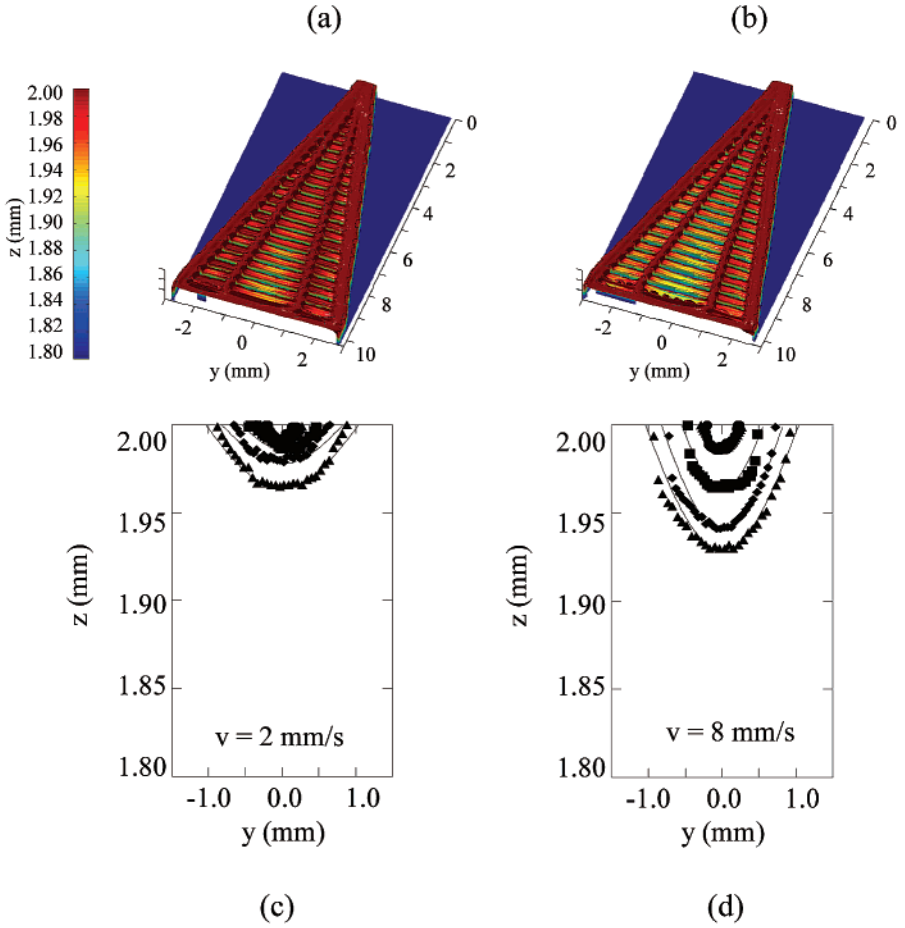

Figure 5. (a−b) Height profiles of test structures from the strongest gel-based ink (pH = 6.15) deposited at speeds of (a) 2 and (b) 8 mm/s. The color scale represents heights between 1.8 and 2 mm. (c−d) Select height profiles for spanning elements at x positions of 3 (●), 5 (■), 7 (◆), and 8.5 (▲) mm from structures deposited at (c) 2 and (d) 8 mm/s. The lines in parts c and d are generated from a simply supported beam with distributed load model.

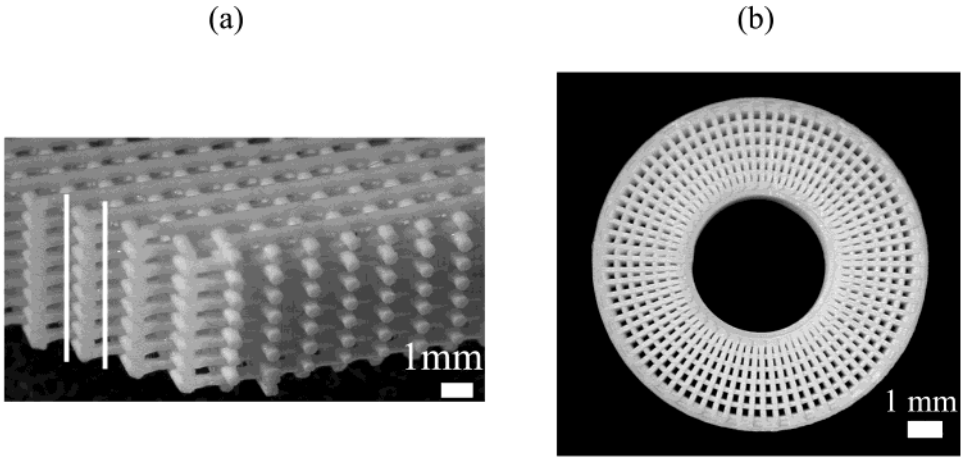

Figure 6. Optical images illustrating (a) a 3-D periodic structure with a simple tetragonal symmetry of lattice rods cut to reveal the high integrity interfaces formed between layers and (b) a 3-D radial structure comprised of alternating layers deposited using radial and concentric fill patterns.

for the 2 mm/s profile, where $r_c/R \sim 0.01$. The introduction of the slip layer (dashed curves) again led to a dramatic reduction in $\dot{\gamma}_{wall}$ (~0.8 to 5 s^{-1}) and an expanded core region ($r_c/R \sim 0.08-0.3$) with decreasing deposition speed.

Shape Evolution of Spanning Structures. The physical geometry of spanning elements resembles that of a beam with circular cross section simply supported at its ends, which deflects in proportion to the distributed load of its own weight as a function of distance from the supports given by[42]

$$\delta z = \frac{Wy}{24EI}(2Ly^2 - y^3 - L^3) \qquad (8)$$

where W is the distributed load ($=0.25[\rho_{gel} - \rho_{oil}]g_0\pi D^2$), ρ_{gel} is the gel density (~4.10 g/cm^3), ρ_{oil} is the oil density (~0.762 g/cm^3), g_0 is the gravitational constant, y is the position along the rod, E is the Young's modulus of the gel

(42) Shigley, J. E.; Mischke, C. R. *Mechanical Engineering Design*, 5th ed.; McGraw-Hill: New York, 1989.

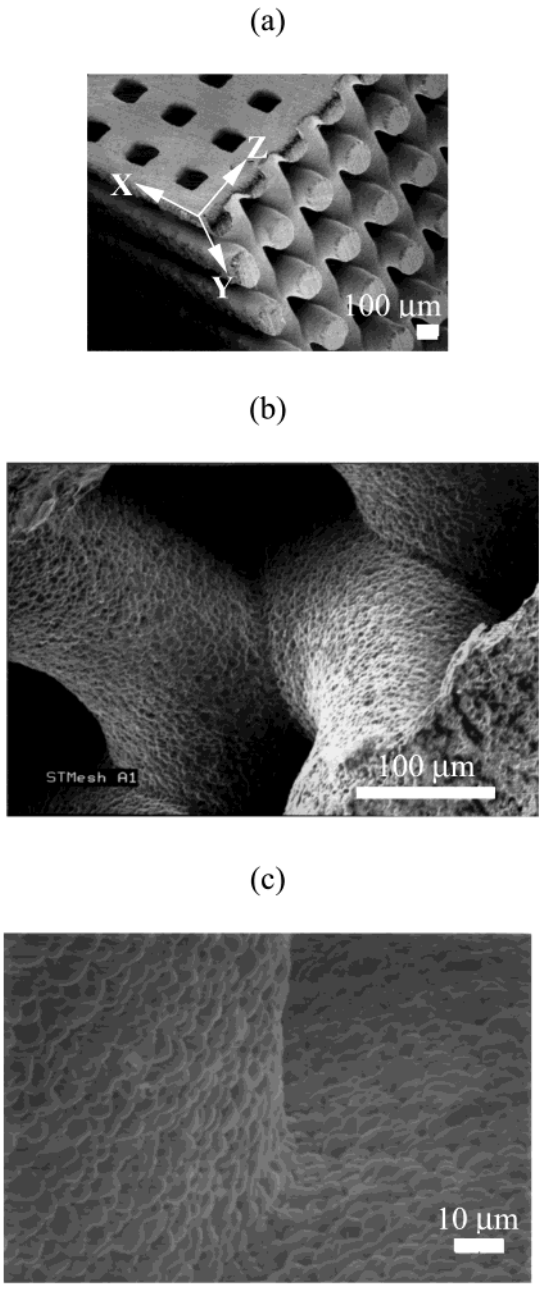

Figure 7. Scanning electron micrographs of a 3-D periodic structure taken at varying magnifications. Image a illustrates the connectivity of the PZT rods in all three dimensions, image b illustrates the bonding that occurs between deposited rods, and image c depicts the surface roughness observed along the rod surfaces, which scales with the characteristic grain size (~5 μm) of the sintered microstructure.

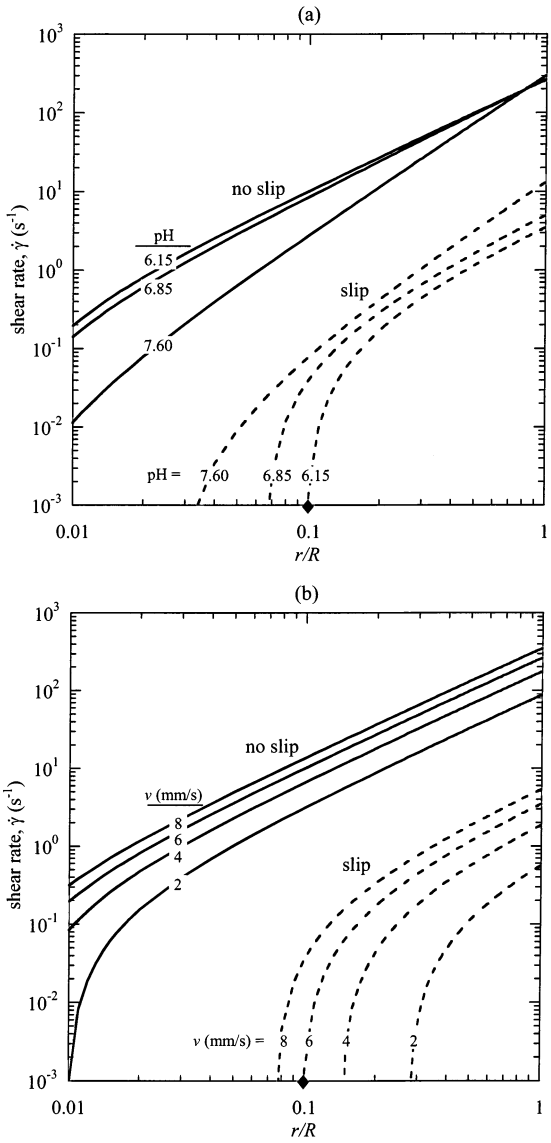

Figure 8. Calculated shear rate profiles for colloidal gel-based inks of varying pH deposited through a cylindrical nozzle (D = 200 μm) at a deposition speed of 6 mm/s assuming (a) a no-slip condition at the nozzle wall and (b) a 0.65 μm slip layer at the nozzle wall.

($E = (1 + 2\nu)G'$),[42] $\nu = 0.5$ is Poisson's ratio for the gel,[20] and I is the area moment of inertia of the circular cross section ($=\pi D^4/64$). Therefore, the modulus, moment of inertia, and distributed load may be used as variable parameters in eq 8 to fit the measured deflection profile of a specific span and capture the elastic properties of the beam. The elimination of drying by assembly in the oil bath fixes the distributed load for these spanning elements; therefore, deflection profiles may be fit by one of two idealized cases: In case 1, an effective homogeneous modulus (G'_{eff}) is selected for the spanning rod and I is held constant. Or in case 2, all the rigidity of the rod is attributed to its core region, whose elastic modulus is given by G'_{eq}, where I is reduced to reflect the core radius.

The static, simply supported beam model is an idealized view of the spanning phenomena, and possible discrepancies with the actual spanning elements should be addressed. During the deposition of the spanning elements, the rod first anchors to one of the supports, traverses the gap, and then anchors to the second support. The deposited rod is in slight tension while traversing the gap, since the gelled ink must bend 90° upon exiting the nozzle to lie in the $x-y$ plane and the connecting points are the nozzle and the first support. This stress is believed to be small given the highly circular rings observed in Figure 7b even across supports that are separated by several rod diameters. Deformation in the elastic limit would occur instantaneously; however, a short time (approximately a few seconds) was required to obtain an equilibrium shape because of their viscoelastic nature.

The height profiles plotted in Figures 4f−h and 5c−d were first fit with eq 8 using a G'_{eff} selected to match the midspan deflection (i.e., $y = L/2$) observed for representative spanning elements from each test structure. These data are shown in Figure 9. The test structure assembled

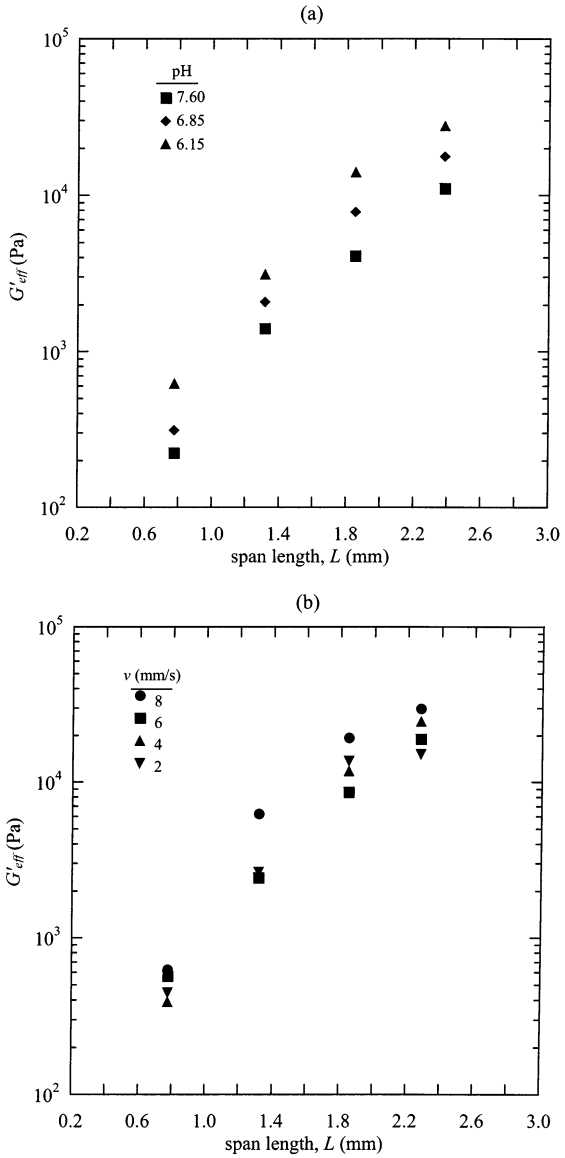

Figure 9. Effective shear modulus (G'_{eff}) required to fit the deflection profiles for selected spans of varying length (L) using the simply supported beam model for structures assembled at a (a) constant deposition speed of $v = 6$ mm/s from colloidal inks of varying pH and (b) varying deposition speed from the strongest gel-based ink (pH = 6.15).

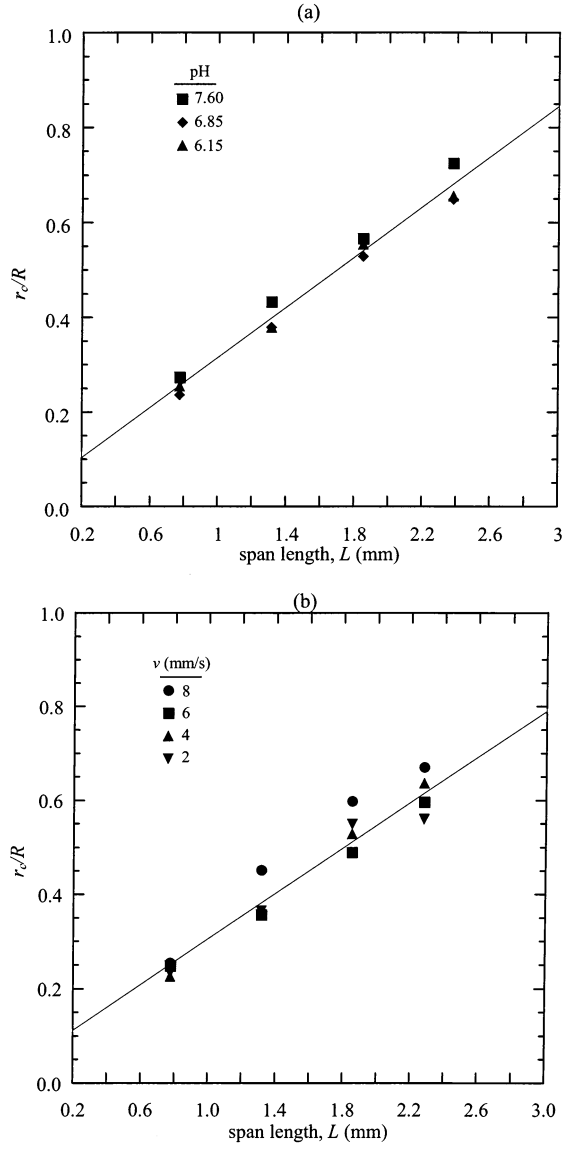

Figure 10. Normalized core radius (r_c/R) required to fit the deflection profiles for selected spans of varying length (L) using a simply supported beam model for structures assembled at a (a) constant deposition speed of $v = 6$ mm/s from colloidal inks of varying pH and (b) varying deposition speed from the strongest gel-based ink (pH = 6.15). In both cases, the line is a linear fit of the average r_c/R as a function of span length.

from the weakest gel (see Figure 4e) was not analyzed further because of the massive deflections observed even at modest span lengths. Profiles from the other test structures revealed that deformation increased with decreasing gel strength and increasing span length, as shown in Figure 4f−h. The G'_{eff} value required to fit the data at a fixed span distance increased with increasing gel strength, as shown in Figure 9a. Interestingly, the value of G'_{eff} required to fit these data increased with span distance for structures assembled from a given gel-based ink. This latter observation implies that the ink becomes more rigid as it spans larger gaps. In fact, the normalized increase in G'_{eff} ($=G'_{eff}/G'_{eq}$) is nearly identical for inks of varying gel strength at a given span distance. This observation suggests that the rate at which these inks become more rigid is nearly independent of their initial elasticity. G'_{eff} was likewise found to increase with increasing span distance for structures assembled from the strongest ink at various deposition speeds, as shown in Figure 9b. There was a modest effect of deposition speed on G'_{eff}, with structures fabricated at higher speed exhibiting a slight reduction in G'_{eff} at a given span length.

The height profiles shown in Figures 4f−h and 5c and d were also fit using the second idealized view, a core−shell composite architecture, for the spanning elements. The core with radius r_c was assigned an elastic modulus equivalent to that of the unyielded gel (G'_{eq}), whereas the fluid shell (which cannot support a static stress) was not assigned a G' value. The G'_{eff} and r_c values required to fit a specific span profile are related by

$$r_c = R\left(\frac{G'_{eff}}{G'_{eq}}\right)^{0.25} \tag{9}$$

The normalized core radius (r_c/R), which is plotted as a function of span length in Figure 10a, appears to be insensitive to gel strength for a given span length. This core region grew linearly with span length, with an extrapolated linear fit of these data yielding an $r_c/R =$

0.10 at $L = 0.2$ mm (i.e., no gap between the supports). Likewise, the core radius appeared to be relatively insensitive to deposition speed at a given L, as shown in Figure 10b; however, a larger scatter in the data was observed as span length increased. The core radius again grew linearly with span length, such that $r_c/R = 0.11$ at $L = 0.2$ mm. The r_c/R values at $L = 0.2$ mm for both cases are marked on the shear rate profiles in Figure 8 by the diamond symbol located on the r_c/R axis. These initial core radii are in excellent agreement with those predicted by the shear rate profiles calculated assuming a slip layer boundary condition. The coincidence of r_c/R data regardless of the gel strengths and deposition speeds studied as well as their linear dependence on span length is a striking result, which may indicate the presence of slip layer variations between these inks. Clearly, this observation requires further analysis.

Core Growth. The apparent growth of the core region as a function of span distance can be explained by the regrowth of a gel network at the core−shell interface. This assertion is based on an observation by Rueb and Zukoski,[21] that the rate of network regrowth in a ruptured colloidal gel increases with the size of residual clusters present at the cessation of flow. The gel structure in the shell region is disrupted by the shear rates experienced in the nozzle, which change as a function of position (see Figure 8). The gel network in the core region percolates along the length of the deposited rod, and therefore, growth in the annular region at the core−shell interface immediately and efficiently enhances the rigidity of a given rod, since $I \propto r_c^4$ (i.e., $\delta z \propto r_c^{-4}$). The data shown in Figure 10 indicate that core growth occurs rapidly (∼1 s), that is, within the time frame of traversing the gap between rods in the underlying layer. This is in good agreement with their characteristic flocculation time of ∼1.7 s estimated using the Smoluchowski approximation.[43] Such observations led to the conclusion that the inks adopt a rigid (gel) core−fluid shell architecture during assembly, with an initial core size that is roughly 10% of the rod diameter.

Implications on Ink Design. The minimum ink elasticity required to assemble a given periodic structure can be estimated by setting a criteria for the maximum acceptable deflection of $\delta z \leq 0.05D$ for $y = L/2$ and rearranging eq 8:

$$G' \geq 1.4\gamma s^4 D \tag{10}$$

where γ is the specific weight of the ink ($=0.25[\rho_{gel} - \rho_{oil}]g_0$) and s is the reduced span distance ($=L/D$). Stronger inks must be formulated as the effective ink density, rod diameter, and normalized span distance increase. These parameters are independent of colloid size, polydispersity, and morphology; therefore, colloidal inks can be created from a broad array of particulate materials (e.g., ceramic, metallic, and polymeric colloids). It may be possible to assemble 3-D periodic structures with much finer features (<100 μm) by developing nanoparticle gels with suitable elasticity. However, such gels must have sufficient nanoparticle volume fraction and strength to minimize drying-induced shrinkage.

Conclusions

A new route for assembling 3-D periodic structures at mesoscopic length scales from colloidal inks has been demonstrated. Concentrated colloidal gels with the appropriate viscoelastic behavior were directly deposited to form spanning structures with characteristic feature sizes ranging from ∼100 μm to 1 mm. Colloidal ink dynamics played an important role in their ability to retain shape upon deposition. This approach opens up an unexplored route for engineering complex 3-D structures from colloidal building blocks, which may find application as advanced ceramics, sensors, composites, and tissue engineering scaffolds.

Acknowledgment. We thank Q. Li and J. Stuecker for their experimental assistance, C. Zukoski for valuable discussions, and B. A. Tuttle and S. Y. Lin for their support. J.A.L. acknowledges partial support from the U.S. Department of Energy, Division of Materials Sciences, through the Frederick Seitz MRL at UIUC. This work was funded by the National Science Foundation (Grant Nos. DMI 99-01030 and DMI 00-99360) and by Sandia, a multiprogram laboratory operated by Sandia Corporation, a Lockheed Martin Company, for the United States Department of Energy under Contract DE-AC04-94AL85000.

LA0257135

(43) Hunter, R. J. *Foundations of Colloid Science*; Oxford University Press Inc.: New York, 1992; Vol. 1.